Shielding Characteristics of Neutron-Shielding Materials in a Cask Structure

K. Ueki, A. Ohashi, N. Nariyama
Ship Research Institute

S. Hode, S. Hattori
Central Research Institute of Electric Power Industry

S. Nagayama, T. Fujita
Genden Engineering Services & Construction Co.

K. Hattori, Y. Anayama
Sanoya Industry Co., Ltd.

INTRODUCTION

Many shielding experiments and analyses have been reported on the shielding effect of materials, and some benchmark or mock-up experiments have been carried out to examine the shielding effects of the specified materials. However, there is no systematic experiment or analysis on the shielding assessment of the materials. The systematic shielding assessment consists of evaluating not only the shielding effects of the material alone but also the effects of combination with other materials and constructing the optimum shielding arrangement with structural materials. In a spent-fuel shipping cask shielding materials are not used alone but are employed with constructional materials such as steel or stainless steel. Accordingly, it is important to investigate the shielding effects not only for the material but also for an arrangement with other materials. Furthermore, the construction of the shielding optimization bring the weight-mitigation of a fabric.

Prior to the present work, Ueki and Namito carried out the shielding experiments using iron and polyethylene shields with a ^{252}Cf neutron source to find an optimum arrangement to minimize neutron and total dose-equivalent rates (Ueki and Namito, 1987, 1989). The total dose-equivalent rate is composed of neutron and secondary gamma-rays.

In this study, the three types of experiments are proposed as a systematic shielding effect of neutron shielding materials. Type 1 is for each shielding material alone, Type 2 is the combination of a neutron shielding material and a structural material, and Type 3 is to constructing the shielding optimization with the materials used in the Type 2 experiment. Especially, due to carry out the Type 2 experiment and analyze it by the Monte Carlo calculation, the acceleration effect of the structural materials, such as steel or stainless steel, which is located to the source side is cleared to the shielding materials located to the detector side.

SHIELDING MATERIALS

The shielding materials examined in this study are summarized in Table 1. Those materials have following shielding characteristics:

1 Polyethylene
The most popular solid neutron shield. However, a lot of secondary gamma-rays are produced by

H (n, γ) reaction of thermal neutrons. The softening temperature is low at 40℃.

2 Water

The most popular liquid neutron shield. However, it is vaporized at 100℃ and also a lot of secondary gamma-rays are produced by thermal neutrons.

3 SUS-304 (Stainless Steel)

The most popular structural material. It has good shielding ability for gamma-rays, but not for neutrons. However, the fast neutrons are slowed down to the keV energy region by inelastic-scattering and make multi-scattering in the energy region. Those energy neutrons are shielded more easily than that of fast neutrons. Accordingly, it is expected that the stainless steel located at the source side serves as an accelerator that reinforces the shielding effects to the following materials.

4 Resin-F

The Resin-F is a kind of synthetic resin containing boron to reduce the production of the secondary gamma-rays by thermal neutrons, and it has been employed in vitrified high-level-wastes shipping casks in France.

5 NS-4-FR

The NS-4-FR is a kind of epoxy resin containing boron to reduce the production of the secondary gamma-rays, and it may be employed in high-burnup spent-fuel shipping casks in Japan.

6 KRAFTON-HB

The KRAFTON-HB is a kind of synthetic resins contained boron to reduce the production of the secondary gamma-rays, and it has been developed for a FBR in the future. The melting point is more than 200℃.

EXPERIMENTS

The neutron shielding experiments with special shielding materials such as Resin-F, NS-4-FR, and KRAFTON-HB, and popular materials such as polyethylene and SUS-304 stainless steel, were carried out by using a ^{252}Cf neutron source of average energy of 2.35 MeV; the source strength was $5.45 \sim 5.33 \times 10^7$ n/s at the experiments. The experimental arrangement of the neutron source, shields, and dosimeter is shown in Fig. 1. The source neutrons were emitted in a cone angle of 45 degrees. The shielding materials were set between the source collimator and the neutron survey meter and the number of the slab shields was increased toward the source side. The size of the slab shields was 80 cm $\times$ 80 cm $\times$ 5 cm thick. The neutron dose-equivalent rates were measured by an ALOKA moderator-type neutron survey meter located 15 cm from the rear-end surface of the shield. The secondary gamma-ray dose-equivalent rates were also measured by an ALOKA scintillation-type survey meter located 5 cm behind the shield. In order to calculate the net dose-equivalent rates from the experiments, both the neutron and the secondary gamma-ray doses were measured by opening the source collimator and closing it at every slab thickness. Then, the net doses were obtained by subtracting the doses measured with the polyethylene cone from those without the cone.

As shown is Fig. 1, the three types of experiments were carried out in this study. Each of the experiments have the following characteristics.

Type 1: In order to investigate the shielding effects of the material alone, the Type 1 experiment was carried out.

Type 2: Neutron shielding effects of the material depend not only on the properties of the material itself but also on which materials are close up. In the present experiments, one case, the SUS-304 stainless steel was located at the source side of the shielding material and in another case, it was at the detector side of the shielding material.

Type 3: This is an expanded arrangement of the Type 2 and nearer to the actual shielding

construction of spent fuel shipping casks. Moving the hydrogenous material from the source side to the detector side, the optimum shielding arrangement for the total dose-equivalent rate (neutron + gamma ray) is obtained. The contribution of the primary gamma rays from the ^{252}Cf source is not observed by the total thickness of 25-cm stainless steel slabs, at the detector location.

TENTH-LAYER FOR NEUTRONS

The tenth-layer for the shielding materials obtained from the present experiments are summarized in Table 2. For water, the data are not from the experiments but from the Monte Carlo calculation.

As expected, polyethylene has the best shielding ability for the ^{252}Cf neutrons among them, and the tenth-layer is 12.5 cm. Polyethylene contains the biggest concentration of hydrogen (14.4 w/o) among them. Even though the weight percent of hydrogen is relatively large ; [Resin-F (4.76 w/o), NS-4-FR (5.92 w/o), and KRAFTON-HB (10.66 w/o)], so as to consider the density of those materials, there is no essential difference of the atomic density of hydrogen, and the tenth-layer is 14.5~15.0 cm. The tenth-layer of water is 16.5 cm by the Monte Carlo calculation, and it is a little bit larger than the other materials. Water has the biggest oxygen concentration (88.81 w/o), but there is no carbon in it. Accordingly, the neutron energy loss by a elastic scattering is less than that of the other materials. The SUS-304 stainless steel itself has little shielding effects, and the tenth-layer is 37.5 cm. However, it has very large resonance elastic-scattering in the keV region and also has considerably large inelastic scattering cross sections in the MeV region. Accordingly, the neutrons penetrated through the thick stainless steel will make a large peak in the keV region.

Table 1. Atomic density of shielding materials.

Element	Polyethylene 0.92 (g/cm^3)	Resin-F 1.81 (g/cm^3)	NS-4-FR 1.68 (g/cm^3)	KRAFTON-HB 1.08 (g/cm^3)	Water 1.0 (g/cm^3)	SUS-304 7.9 (g/cm^3)
	(w/o)	(w/o)	(w/o)	(w/o)	(w/o)	(w/o)
Hydrogen	14.4	4.76	5.92	10.66	11.19	
Boron		0.9	0.94	0.78		
Carbon	85.6	23.10	27.63	75.29		
Nitrogen			1.98	2.20		
Oxygen		48.95	42.29	10.69	88.81	
Aluminum		21.40	21.24			
Silicon				0.38		1.00
Chromium						20.00
Manganese						2.00
Iron						66.5
Nickel						10.5
Zinc		1.82				

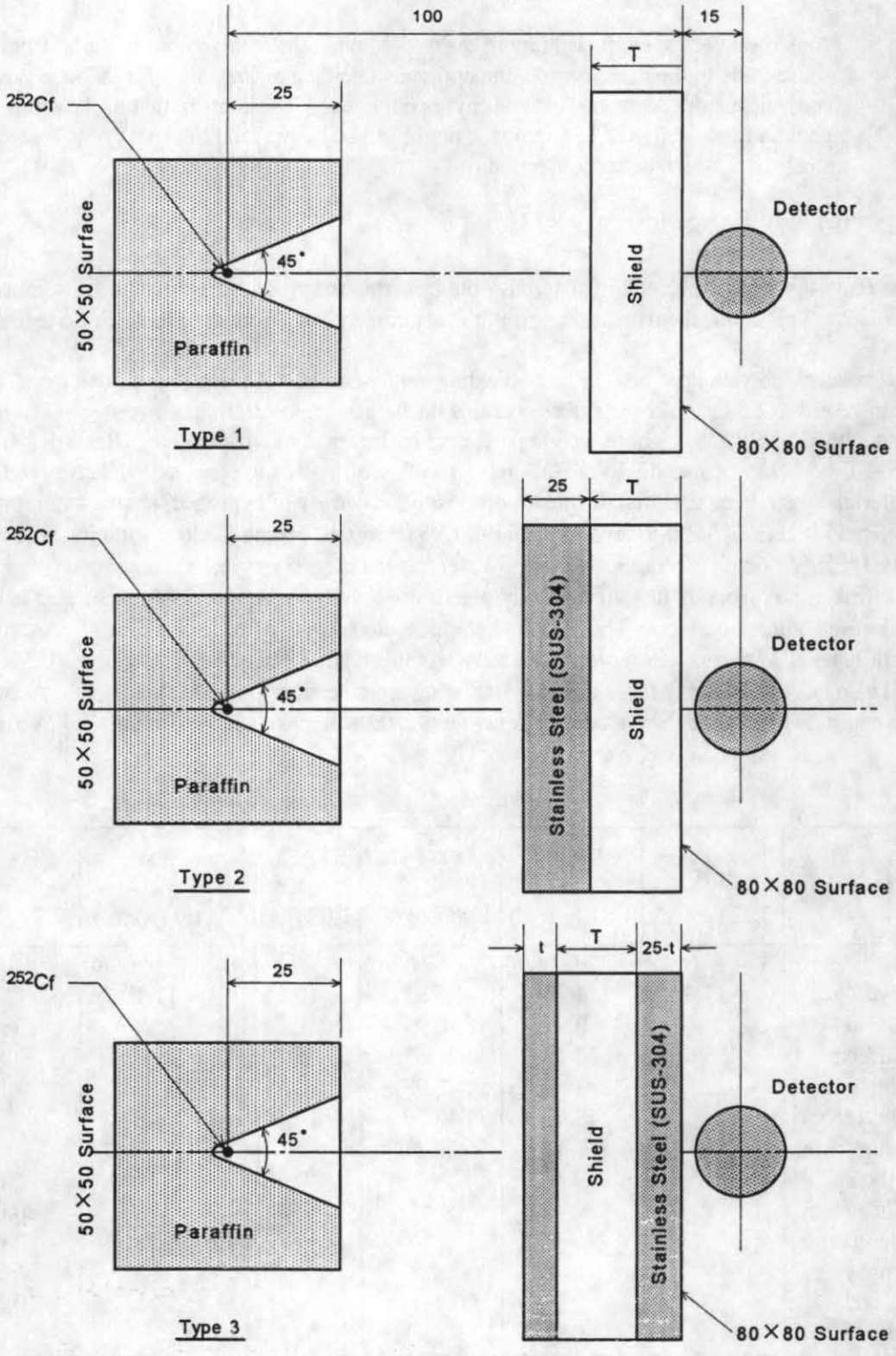

Fig.1. Schematic arrangement of source, shields, and detector. Dimensions are all in centimetres. The T is thickness of a shield. Type 1 is only shielding material, Type 2 is a shielding arrangement of SUS-304 and shield slabs, and Type 3 is a shielding arrangement of SUS-304+shield+SUS-304 slabs.

Table 2. The tenth-layer of neutron dose-equivalent rate for shielding materials to ^{252}Cf neutrons, obtained by the experiments.

Shielding Materials	Tenth-Layer (cm)
Polyethylene	12.5
Resin-F	15.0
NS-4-FR	14.5
KRAFTON-HB	14.5
Water	16.5 (Calculation)
SUS-304	37.5

MONTE CARLO ANALYSES AND DISCUSSIONS

Monte Carlo Techniques

The experiments were analyzed by the continuous energy Monte Carlo code MCNP 4A (Briesmeister, 1993) with the neutron cross sections of JENDL 3.2 (Japanese Evaluated Nuclear Data Version 3.2) (Shibata, et al., 1990). In order to do effective Monte Carlo analysis for the present experiments, the NESX (Next Event Surface Crossing) estimator was employed. The NESX estimator is not provided in the MCNP 4A code. Therefore, instead of the point detector estimator, the NESX estimator was newly built in the subroutine TALLYD of the MCNP 4A code.

Acceleration Effects by Stainless Steel

Figure 2 shows the experiments and Monte Carlo calculations of the dose-equivalent rate attenuation profiles for the source side of polyethylene + detector side of SUS-304 and the reverse arrangement of the Type 2 experiment in Fig. 1.

As expected, the SUS-304 + polyethylene arrangement shows much better shielding effects than that of the polyethylene + SUS-304 shielding arrangement by the accelerating effects of stainless steel. In order to explain the accelerating effects of stainless steel, the difference of the neutron energy spectra on the source side surface and on the detector side surface of the 25-cm thick SUS-304 shield were calculated by the Monte Carlo code MCNP 4A. Noticeable points are that the peak of the energy spectrum is approximately 1 MeV on the source side, and it is approximately 0.4 MeV on the detector side, and the ratio of the fast neutrons (> 1 MeV) on the detector side surface is obviously less than that of the source side. In consequence, those neutrons of the keV energy region are shielded easily by the polyethylene slabs in the SUS-304 + polyethylene arrangement. However, fast neutrons of the ^{252}Cf source are entered into the polyethylene slabs directly in the polyethylene + SUS-304 arrangement. Those fast neutrons cannot shield easier than that of the keV energy region.

Based on the experimental data, the tenth-layer of the polyethylene slabs in the SUS-304 + polyethylene arrangement is 7 cm, and it is 12 cm in the polyethylene + SUS-304 arrangement. The tenth-layer of 7 cm is approximately half of the polyethylene alone. As described before, the stainless steel located at the source side serves as an accelerator for the polyethylene following it. On the other hand, there is no essential difference between the polyethylene + SUS-304 arrangement and the polyethylene alone.

As shown in Fig. 3, the neutron shielding material of a cask is located out of the structural steel in general. Therefore, the structure is to be reasonable not only from the weight minimization but also from the shielding optimization point of view, too. The shielding system of the TN-12A spent-fuel shipping cask in Fig. 3 is that the 30-cm thick steel is located at source side and the 10-cm thick resin is outside.

In the polyethylene + SUS-304 shielding arrangement, the Monte Carlo calculations are overestimated as the thickness of the polyethylene slabs is increased; however, the calculations are underestimated as the thickness of the polyethylene slabs is increased in the SUS-304 + polyethylene shielding arrangement.

Optimum Shielding Arrangement

Finding the optimum shielding arrangement, neutron and secondary gamma-ray dose-equivalent rates were measured in the polyethylene-stainless steel shielding arrangement of the Type 3 experiment in Fig. 1. The measured data are summarized in Fig. 4. The Monte Carlo calculations were also carried out by the MCNP 4A for the neutron and secondary gamma-ray dose-equivalent rates.

The neutron dose-equivalent rate decreases as the polyethylene slab of 15-cm thick is moved to the detector side. On the other hand, the secondary gamma-rays dose increases as the polyethylene slab is moved to the detector side. As a consequence, the minimum dose point is built up at the t is 20 cm of the Type 3 experiment in Fig. 1. That is, the 20-cm thick SUS-304 slab is located at the source side of the polyethylene, and the 5-cm thick SUS-304 slab is at the detector side of the polyethylene. This arrangement of the 20-cm thick stainless steel + 15-cm thick polyethylene + 5-cm thick stainless steel is the optimum arrangement for the stainless steel-polyethylene shielding system. The ratio of the minimum total dose-equivalent rate (neutron + secondary gamma-ray) to the maximum one is 2.5. In conclusion, even though the total thickness of the shielding system is constant, the total dose-equivalent rate can be reduced by a factor of 2.5 as compared with the pessimistic arrangement by making the optimum arrangement.

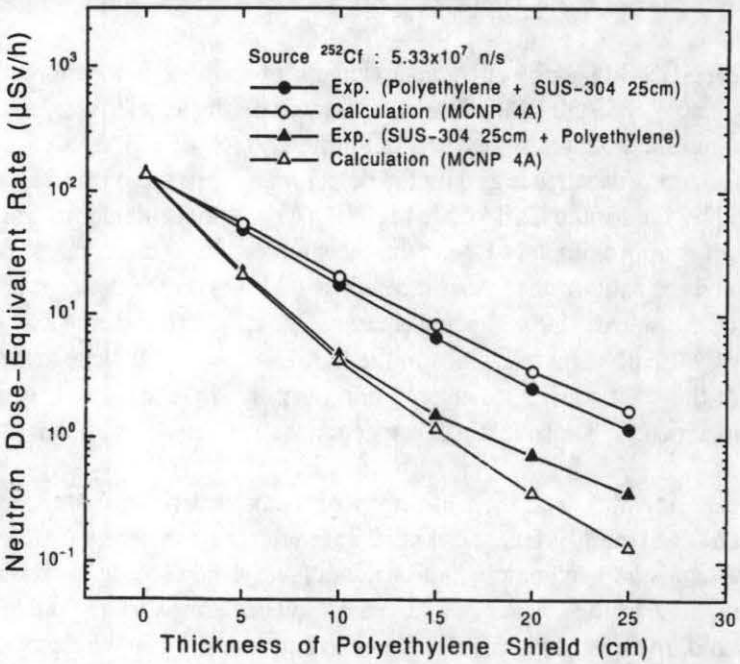

Fig.2 Difference of dose-equivalent rate attenuation profile between polyethylene+SUS-304 and SUS-304+polyethylene slabs arrangement of Type 2 experiment in Fig.1.

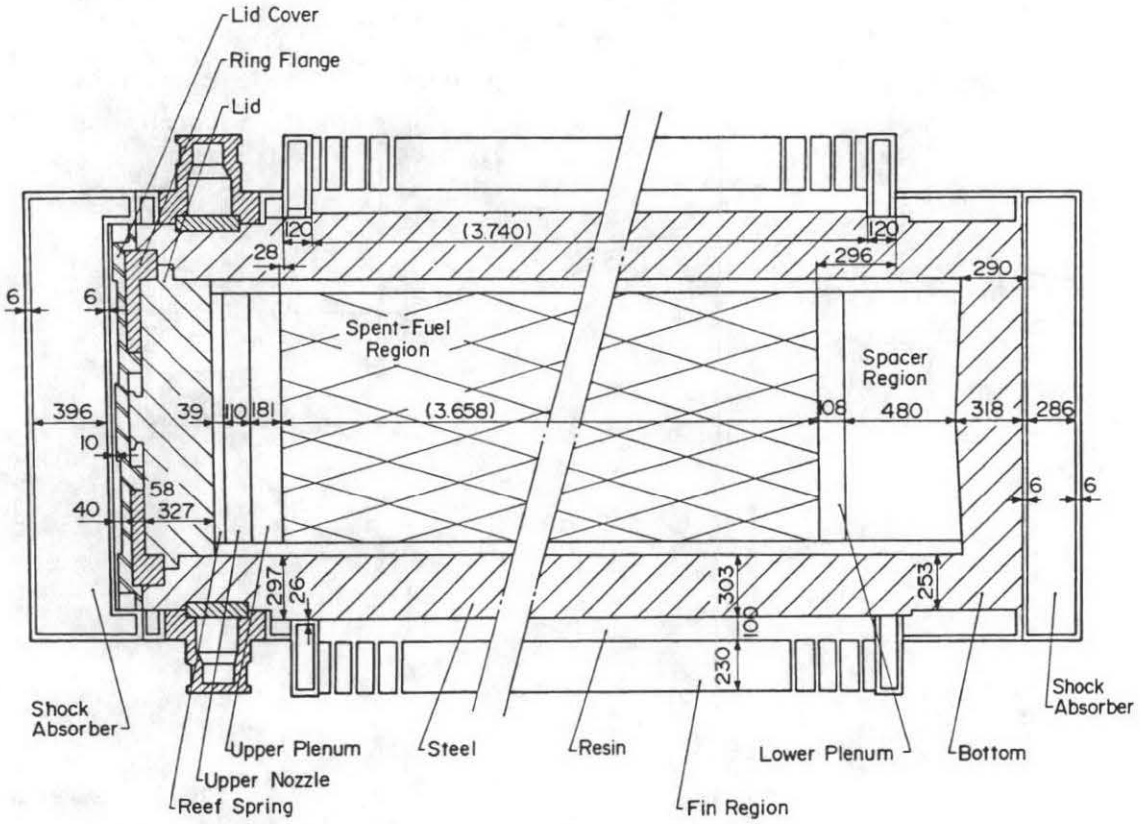

Fig. 3 Shielding structure of the TN-12A cask. Dimensions are in centimeters.

CONCLUSIONS

The following remarks are obtained from the present experiments and the Monte Carlo analysis.

1. The systematic assessment of a shielding material is performed by conducting all of the Type 1, Type 2, and Type 3 experiments.
2. Shielding ability of individual materials is evaluated by the Type 1 experiment. Polyethylene is the best and Resin-F, NS-4-FR, and KRAFTON-HB are a little worse than that of polyethylene but better than that of water.
3. The accelerating effects of non-hydrogenous materials can be established by the Type 2 experiment. The effects are remarkable, and the tenth-layer of the polyethylene slab followed by the stainless steel becomes approximately half of using it alone.
4. The optimum shielding arrangement for the total dose-equivalent rate can be found by the Type 3 experiment. The dose-equivalent rate ratio of the optimum arrangement to the pessimistic arrangement is more than the factor of 2.5. The shielding system of a spent-fuel shipping cask is to be reasonable from the shielding optimization point of view.
5. The Monte Carlo calculations with the NESX estimator can reproduce the experimental results fairly well. Accordingly, the Monte Carlo calculation can be employed as an alternative assessment method in lieu of the systematic assessment of a shielding material.

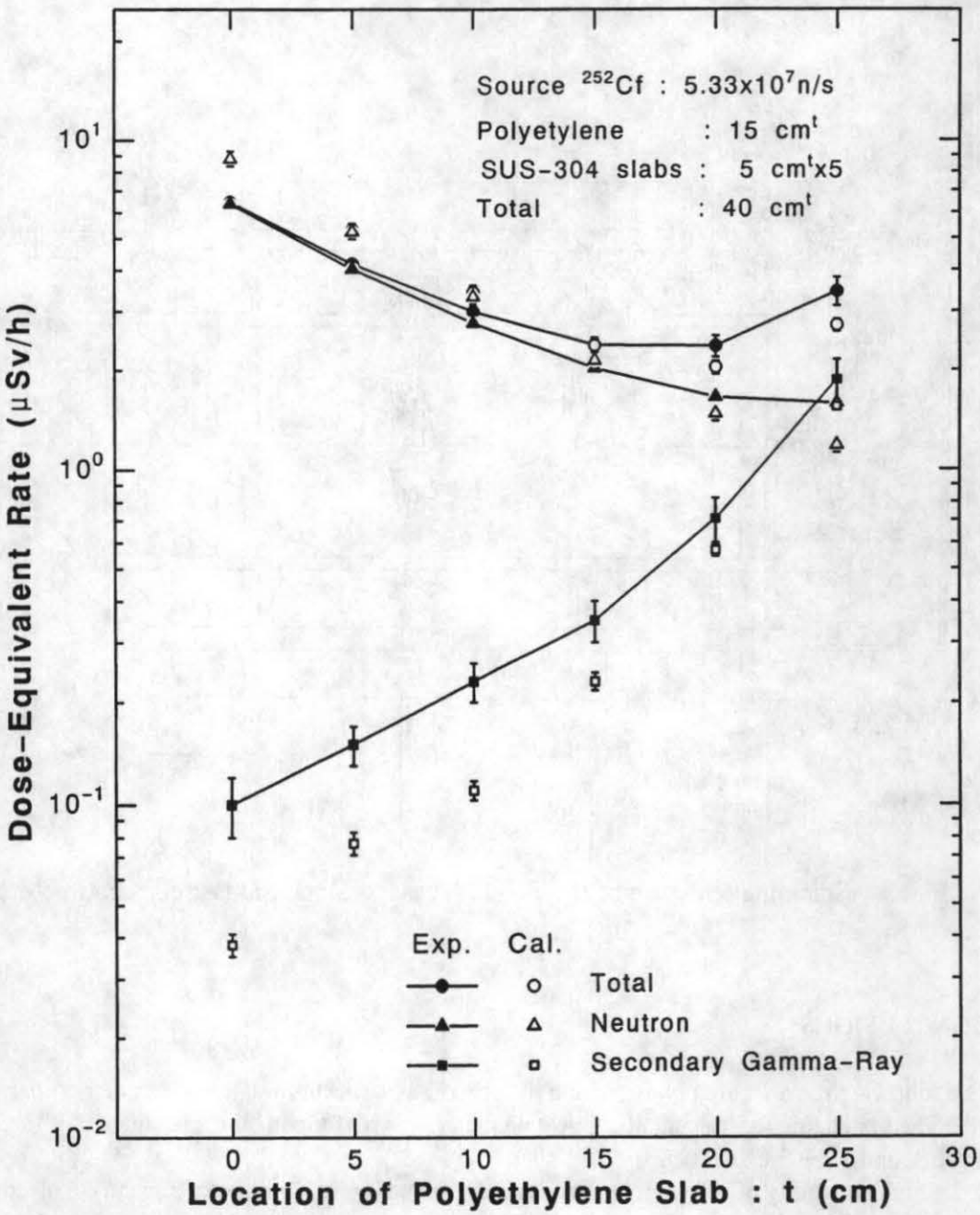

Fig.4 Comparison of measured and Monte Carlo analysis for shielding optimization of the SUS-304-polyethylene arrangement with ^{252}Cf neutron source. The t is a distance of the Type 3 in Fig.1.

REFERENCES

Briesmeister, J.F., Editor *MCNP™-A General Monte Carlo N-Particle Transport Code, Version 4A*, Los Alamos National Laboratory, LA-12625-M (1993).

K. Shibata, et al. *Japanese Evaluated Nuclear Data library, Version 3*, JAERI-1319, Japan Atomic Energy Research Institute (1990).

K. Ueki, Y. Namito, Nucl. Sci. Eng., 96, 30(1987).

Idem: J. Nucl. Sci. Technol., 26 [4] 411 (1989).